RIS-AIDED MONOSTATIC MIMO RADAR WITH CO-LOCATED ANTENNAS

Stefano Buzzi[*], *Emanuele Grossi*[*], *Marco Lops*[†], *Luca Venturino*[*]

[*]DIEI, University of Cassino and Southern Lazio, Italy & CNIT, Italy
[†]DIETI, University of Naples Federico II, Italy & CNIT, Italy

ABSTRACT

This paper considers a monostatic multiple-input multiple-output (MIMO) radar aided by a reconfigurable intelligent surface (RIS). After modeling the received target signal as the superposition of four echoes, which may involve up to two bounces off the RIS, the phases of the reflecting elements and the radar receive filter are chosen to maximize the signal-to-noise ratio (SNR). Some examples are provided to assess the performance of this novel architecture.

Index Terms— MIMO, Monostatic Radar, Reconfigurable Intelligent Surfaces, Metasurfaces.

1. INTRODUCTION

An reconfigurable intelligent surface (RIS) is an emerging technology which promises to push the performance of wireless communication networks well beyond the current boundaries [1, 2]. Recently, their use has been also proposed in the context of radar target detection [3–6]. The studies in [3,4] offer a first investigation of the potential benefits when an RIS is placed in proximity to a monostatic radar, while [5] proposes to use of a far-field RIS as a mirror to extend the field of view of a scanning radar. Finally, the study in [6] considers a general architecture encompassing a multiple-input multiple-output (MIMO) radar with co-located antennas, in a monostatic or a bistatic configuration, wherein the transmitter and/or the receiver can exploit a nearby RIS to illuminate and observe a prospective target; here, the system parameters are designed to maximize the detection probability at a given location under inspection, and the impact of the radar-RIS distance and the RIS size are studied. The major findings of these initial works are that the indirect echoes can be used to modify the radar field of view and that combining the indirect echoes passing trough the RIS with an already-existing direct echo is cost-effective only if the RIS size is sufficiently large to balance the additional path loss in the radar-RIS hop.

The present contribution aims at shedding further light into the use of an RIS in close proximity of a monostatic MIMO radar equipped with closely-spaced antennas. The degrees of freedom for system optimization are the phases of the reflecting elements (assumed to be the same when illuminating and observing the target) and the radar receive filter. After introducing the signal model, we state the system design problem as the maximization of the received signal-to-noise ratio (SNR) at the location under inspection, whose approximate solution is undertaken through an alternate maximization procedure. The analysis shows that a major advantage of the considered architecture is that the RIS and the radar (transmit or receive) array are seen as "co-located" by a target at relatively modest distances. As a consequence, the RIS design ends up with being *independent* of the range and can be undertaken once and for all if the angular direction of interest is defined. The results also indicate that the RIS phases and the radar receive filter can be also focused towards different directions in practice; this is an attractive feature in light of the fact that, while the RIS has to be programmed before the transmission of the probing signal, the radar receiver can be reconfigured to simultaneously form multiple beams. Finally, we show that the resulting beampattern presents some inherent fragility with respect to the mismatch between the nominal and the actual target direction, since direct and indirect echoes may experience a destructive superposition when the actual direction deviates from the nominal one.

This paper is organized as follows. Sec. 2 gives the system description. Sec. 3 studies the design of the phases of the RIS. Sec. 4 gives some numerical examples. Finally, concluding remarks are provided in Sec. 5.

Notation: The superscripts $(\cdot)^*$, $(\cdot)^{\mathsf{T}}$, and $(\cdot)^{\mathsf{H}}$ denote conjugate, transpose, and conjugate-transpose, respectively. $\boldsymbol{I}_M$ is the $M \times M$ identity matrix. $\mathrm{diag}\{\boldsymbol{a}\}$ is the $M \times M$ matrix containing the entries of M-dimensional vector $\boldsymbol{a}$ on the main diagonal and zero elsewhere. The symbol $\otimes$ denotes the Kronecker product and i the imaginary unit.

2. SYSTEM DESCRIPTION

We consider a monostatic radar whose transmitter and receiver are equipped with $\bar{N}_r$ and $\ddot{N}_r$ closely-spaced antennas, respectively. The radar operates with a carrier wavelength λ and emits $\bar{N}_r$ orthogonal and equal-power narrowband waveforms, one from each radiating element. A nearby RIS helps the radar illuminate/observe a prospective point-like target; this surface is composed of N_s closely-spaced reflecting ele-

The work of S. Buzzi, E. Grossi, and L. Venturino was supported by the MIUR program "Dipartimenti di Eccellenza 2018–2022".

ments of area A_s; we denote by φ_n the phase shift introduced by the n-th element, with $\boldsymbol{\varphi} = (\varphi_1 \ \dots \ \varphi_{N_s})^{\mathsf{T}}$.

We make the following design assumptions. The radar and RIS see the same aspect angle of the target [7]; the phase curvature of the wavefront can be neglected in the radar-target and RIS-target hops, but not in the radar-RIS hop [8, 9]; there is line-of-sight (LOS) propagation and no coupling among the radar antennas and the RIS elements; all paths from the radar transmitter to the target to the radar receiver have non-resolvable delays. As illustrated in [6], these assumptions pose constraints on the radar and RIS apertures, the radar-RIS distance, and the target size and range.

Finally, we define the following geometric quantities: d_r, θ_r^{az}, and θ_r^{el} are the range and the azimuth and elevation angles of the target from the radar phase center (common to both the transmit and the receive array), respectively; d_s, θ_s^{az}, and θ_s^{el} are the range and the azimuth and elevation angles of the target from the RIS phase center, respectively; δ, ρ^{az}, ρ^{el}, ω^{az}, and ω^{el} are the length, the azimuth and elevation angles of departure, and the azimuth and elevation angles of arrival in the path from the radar phase center to the RIS phase center, respectively. For brevity, we denote by $\phi = \{\phi^{\mathrm{az}}, \phi^{\mathrm{el}}\}$ the pair of azimuth and elevation angles ϕ^{az} and ϕ^{el}.

2.1. Received signal

A range gating operation is performed by projecting the signal impinging on each receive element along a delayed version of each transmit waveform, with the delay tied to the distance of the inspected location. The $N_r = \ddot{N}_r \bar{N}_r$ data samples are then organized into a vector $\boldsymbol{r} \in \mathbb{C}^{N_r}$ that, in the presence of a steady target, can be modeled as [6]

$$\boldsymbol{r} = \underbrace{\left(\bar{\gamma}_r \bar{\boldsymbol{v}}_r + \bar{\gamma}_s \bar{\boldsymbol{G}} \boldsymbol{X}(\boldsymbol{\varphi}) \boldsymbol{v}_s\right) \otimes \left(\ddot{\gamma}_r \ddot{\boldsymbol{v}}_r + \ddot{\gamma}_s \ddot{\boldsymbol{G}} \boldsymbol{X}(\boldsymbol{\varphi}) \boldsymbol{v}_s\right)}_{\boldsymbol{e}(\boldsymbol{\varphi})} \alpha + \boldsymbol{w} \tag{1}$$

where $\boldsymbol{e}(\boldsymbol{\varphi}) \in \mathbb{C}^{N_r}$ is the *target signature*, tied to the system geometry and the RIS phase shifts, $\alpha \in \mathbb{C}$ accounts for the unknown target response and any other scaling factor not included in $\boldsymbol{e}(\boldsymbol{\varphi})$ (such as, for example, the transmit power); and $\boldsymbol{w} \in \mathbb{C}^{N_r}$ is a circularity-symmetric Gaussian vector with covariance matrix $\sigma_w^2 \boldsymbol{I}_{N_r}$, accounting for the disturbance.

The target signature $\boldsymbol{e}(\boldsymbol{\varphi})$ results from the superposition of four paths from the radar transmitter to the target to the radar receiver, which may involve up to two bounces off the RIS; here, $\bar{\gamma}_r$ and $\bar{\gamma}_s$ are the complex amplitudes of the forward paths from the radar phase center to the target and from the radar phase center to the RIS phase center to the target, respectively, while $\ddot{\gamma}_r$ and $\ddot{\gamma}_s$ are the complex amplitudes of the corresponding backward paths; from the radar equation [10], we have

$$\bar{\gamma}_r = \left(\frac{\bar{\mathcal{G}}(\theta_r)}{4\pi d_r^2}\right)^{1/2} e^{-\mathrm{i}2\pi d_r/\lambda} \tag{2a}$$

$$\bar{\gamma}_s = \left(\frac{\bar{\mathcal{G}}(\rho)\zeta(\omega, \theta_s)}{(4\pi)^2 \delta^2 d_s^2}\right)^{1/2} e^{-\mathrm{i}2\pi(\delta + d_s)/\lambda} \tag{2b}$$

$$\ddot{\gamma}_r = \left(\frac{\ddot{\mathcal{G}}(\theta_r)\lambda^2}{(4\pi)^2 d_r^2}\right)^{1/2} e^{-\mathrm{i}2\pi d_r/\lambda} \tag{2c}$$

$$\ddot{\gamma}_s = \left(\frac{\ddot{\mathcal{G}}(\rho)\zeta(\theta_s, \omega)\lambda^2}{(4\pi)^3 \delta^2 d_s^2}\right)^{1/2} e^{-\mathrm{i}2\pi(\delta + d_s)/\lambda} \tag{2d}$$

where $\bar{\mathcal{G}}(\phi)$ and $\ddot{\mathcal{G}}(\phi)$ are the gain of the transmit and receive antennas of the radar towards ϕ, respectively, and $\zeta(\phi_i, \phi_o)$ is the bi-static radar cross-section (RCS) of a reflecting element towards $\phi_o = \{\phi_o^{\mathrm{az}}, \phi_o^{\mathrm{el}}\}$ when illuminated from $\phi_i = \{\phi_i^{\mathrm{az}}, \phi_i^{\mathrm{el}}\}$;[1] $\bar{\boldsymbol{v}}_r \in \mathbb{C}^{\bar{N}_r}$ and $\ddot{\boldsymbol{v}}_r \in \mathbb{C}^{\ddot{N}_r}$ are the *direct* transmit and receive steering vectors of the radar towards the target, respectively; $\boldsymbol{v}_s \in \mathbb{C}^{N_s}$ is the steering vector of the RIS towards the target; $\boldsymbol{X}(\boldsymbol{\varphi}) = \mathrm{diag}\{(e^{\mathrm{i}\varphi_1} \ \cdots \ e^{\mathrm{i}\varphi_{N_s}})^{\mathsf{T}}\} \in \mathbb{C}^{N_s \times N_s}$; $\bar{\boldsymbol{G}} \in \mathbb{C}^{\bar{N}_r \times N_s}$ is the (normalized) channel matrix between the radar transmitter and the RIS, whose entries are [11]

$$\bar{G}_{jn} = \left(\frac{\bar{\mathcal{G}}(\bar{\rho}_{jn})\zeta(\bar{\omega}_{jn}, \theta_s)\delta^2}{\bar{\mathcal{G}}(\rho)\zeta(\omega, \theta_s)\bar{\delta}_{jn}^2}\right)^{1/2} e^{-\mathrm{i}2\pi(\bar{\delta}_{jn} - \delta)/\lambda} \tag{3}$$

where $\bar{\delta}_{jn}$, $\bar{\rho}_{jn}^{\mathrm{az}}$, $\bar{\rho}_{jn}^{\mathrm{el}}$, $\bar{\omega}_{jn}^{\mathrm{az}}$, and $\bar{\omega}_{jn}^{\mathrm{el}}$ are the length, the azimuth and elevation angles of departure, and the azimuth and elevation angles of arrival in the path from the j-th transmit element of the radar to the n-th element of the RIS, respectively, with $\bar{\rho}_{jn} = \{\bar{\rho}_{jn}^{\mathrm{az}}, \bar{\rho}_{jn}^{\mathrm{el}}\}$ and $\bar{\omega}_{jn} = \{\bar{\omega}_{jn}^{\mathrm{az}}, \bar{\omega}_{jn}^{\mathrm{el}}\}$; finally, $\ddot{\boldsymbol{G}} \in \mathbb{C}^{\ddot{N}_r \times N_s}$ is the (normalized) channel matrix between the radar receiver and the RIS, which is defined similarly to $\bar{\boldsymbol{G}}$. Notice that $\bar{\boldsymbol{G}}\boldsymbol{X}(\boldsymbol{\varphi})\boldsymbol{v}_s$ and $\ddot{\boldsymbol{G}}\boldsymbol{X}(\boldsymbol{\varphi})\boldsymbol{v}_s$ can be regarded as the *indirect* transmit and receive steering vectors of the radar towards the target via the RIS-assisted path, respectively.

3. SYSTEM DESIGN

Let $\boldsymbol{f} \in \mathbb{C}^{N_r}$ be the unit-norm receive filter; then, its output is $r = \boldsymbol{f}^{\mathsf{H}} \boldsymbol{e}(\boldsymbol{\varphi})\alpha + \boldsymbol{f}^{\mathsf{H}} \boldsymbol{w}$, resulting in the following SNR

$$\mathrm{SNR} = \left|\boldsymbol{f}^{\mathsf{H}} \boldsymbol{e}(\boldsymbol{\varphi})\right|^2 \sigma_\alpha^2 / \sigma_w^2 \tag{4}$$

where $\sigma_\alpha^2 = \mathrm{E}[|\alpha|^2]$. We propose here to choose $\boldsymbol{f}$ and $\boldsymbol{\varphi}$ so as to maximize the SNR at the inspected location; indeed, a larger SNR also implies as a by product a larger probability of detection and a better estimation accuracy of the unknown target response [12–14]. For any $\boldsymbol{\varphi}$, the optimal receive filter is $\boldsymbol{f} = \boldsymbol{e}(\boldsymbol{\varphi})/\|\boldsymbol{e}(\boldsymbol{\varphi})\|$. Upon plugging this latter expression into (4), the problem to be tackled is

$$\max_{\boldsymbol{\varphi}} \|\boldsymbol{e}(\boldsymbol{\varphi})\|^2. \tag{5}$$

[1] If the transmit and receive antennas of the radar have the same gain, i.e., $\bar{\mathcal{G}}(\phi) = \ddot{\mathcal{G}}(\phi)$, then $\ddot{\gamma}_r = \bar{\gamma}_r \lambda^2/(4\pi)$; in addition, if the RIS is reciprocal, i.e., $\zeta(\phi_i, \phi_o) = \zeta(\phi_o, \phi_i)$, then $\ddot{\gamma}_s = \bar{\gamma}_s \lambda^2/(4\pi)$.

Algorithm 1 Alternate maximization for Problem (5)

Choose $\epsilon > 0$, $K_{\max} > 0$, and $\boldsymbol{\varphi} \in [0, 2\pi]^{N_s}$
$k = 0$ and $f_0 = 0$
repeat
  for $n = 1, \ldots, N_s$ **do**
    $\varphi_n = \arg\max_{\varphi} \Re\{A_n e^{\mathrm{i}\varphi} + B_n e^{\mathrm{i}2\varphi}\}$
  end for
  $k = k + 1$
  $f_k = \|\boldsymbol{e}(\boldsymbol{\varphi}, \boldsymbol{\varphi})\|^2$
until $f_k - f_{k-1} < \epsilon f_k$ or $k = K_{\max}$

Next, we compute a sub-optimal solution to (5) by iteratively optimizing one phase shift at a time. To proceed, the objective function is expanded as

$$\begin{aligned}\|\boldsymbol{e}(\boldsymbol{\varphi})\|^2 &= \left\|\bar{\boldsymbol{t}}_n + \bar{\boldsymbol{q}}_n e^{\mathrm{i}\varphi_n}\right\|^2 \left\|\ddot{\boldsymbol{t}}_n + \ddot{\boldsymbol{q}}_n e^{\mathrm{i}\varphi_n}\right\|^2 \\ &= \left(\|\bar{\boldsymbol{t}}_n\|^2 + \|\bar{\boldsymbol{q}}_n\|^2\right)\left(\|\ddot{\boldsymbol{t}}_n\|^2 + \|\ddot{\boldsymbol{q}}_n\|^2\right) \\ &\quad + 2\left(\|\bar{\boldsymbol{t}}_n\|^2 + \|\bar{\boldsymbol{q}}_n\|^2\right)\Re\left\{\ddot{\boldsymbol{t}}_n^{\mathsf{H}}\ddot{\boldsymbol{q}}_n e^{\mathrm{i}\varphi_n}\right\} \\ &\quad + 2\left(\|\ddot{\boldsymbol{t}}_n\|^2 + \|\ddot{\boldsymbol{q}}_n\|^2\right)\Re\left\{\bar{\boldsymbol{t}}_n^{\mathsf{H}}\bar{\boldsymbol{q}}_n e^{\mathrm{i}\varphi_n}\right\} \\ &\quad + 4\Re\left\{\ddot{\boldsymbol{t}}_n^{\mathsf{H}}\ddot{\boldsymbol{q}}_n\bar{\boldsymbol{t}}_n^{\mathsf{H}}\bar{\boldsymbol{q}}_n e^{\mathrm{i}2\varphi_n}\right\} \end{aligned} \tag{6}$$

where $\bar{\boldsymbol{q}}_n$ is the n-th column of $\bar{\gamma}_s\bar{\boldsymbol{G}}\mathrm{diag}\,(\boldsymbol{v}_s)$, $\bar{\boldsymbol{t}}_n = \bar{\gamma}_r\boldsymbol{v}_r + \sum_{j=1,\,j\neq n}^{N_s}\bar{\boldsymbol{q}}_j e^{\mathrm{i}\varphi_j}$, $\ddot{\boldsymbol{q}}_n$ is the n-th column of $\ddot{\gamma}_s\ddot{\boldsymbol{G}}\mathrm{diag}\,(\boldsymbol{v}_s)$, and $\ddot{\boldsymbol{t}}_n = \ddot{\gamma}_r\ddot{\boldsymbol{v}}_r + \sum_{j=1,\,j\neq n}^{N_s}\ddot{\boldsymbol{q}}_j e^{\mathrm{i}\varphi_j}$. Neglecting the irrelevant terms in (6), the problem to be solved becomes

$$\max_{\varphi_n} \Re\{A_n e^{\mathrm{i}\varphi_n} + B_n e^{\mathrm{i}2\varphi_n}\} \tag{7}$$

where $A_n = 2\left(\|\bar{\boldsymbol{t}}_n\|^2 + \|\bar{\boldsymbol{q}}_n\|^2\right)\ddot{\boldsymbol{t}}_n^{\mathsf{H}}\ddot{\boldsymbol{q}}_n + 2\left(\|\ddot{\boldsymbol{t}}_n\|^2 + \|\ddot{\boldsymbol{q}}_n\|^2\right)\bar{\boldsymbol{t}}_n^{\mathsf{H}}\bar{\boldsymbol{q}}_n$ and $B_n = 4\ddot{\boldsymbol{t}}_n^{\mathsf{H}}\ddot{\boldsymbol{q}}_n\bar{\boldsymbol{t}}_n^{\mathsf{H}}\bar{\boldsymbol{q}}_n$. The solution to (7) can be found among the zeros of the derivative of the objective function, i.e., $|A_n|\sin(\varphi_n + \angle A_n) + 2|B_n|\sin(2\varphi_n + \angle B_n)$. The overall procedure is summarized in Algorithm 1. Since the objective function is bounded above and monotonically increased at each iteration, convergence is ensured.

4. PERFORMANCE ANALYSIS

We assess the system performance for the geometry in Fig. 1, when the carrier wavelength is $\lambda = 10$ cm, the signal bandwidth is 1 MHz, and the target size is 50 cm. Each array is on the (y, z)-plane of a Cartesian local reference system, with elements oriented towards the positive x-axis. The local x and y axes of the transmit, receive, and reflecting arrays lays on the same plane, which also contains the target. The radar employs a linear array with a $\lambda/2$ element spacing along the y-axis and $\bar{N}_r = \ddot{N}_r = 4$; each antenna has a power beampattern with a 3-dB width of 120° in azimuth and of 60° in elevation. The RIS is a square flat surface and contains $N_s = 225$ adjacent elements of area $A_s = \lambda^2/4$. Leveraging [4,6,15–17], the RIS is modeled as a reciprocal surface with $\zeta(\phi_i, \phi_o) = \left[A_s\cos(\phi_i^{\mathrm{az}})\cos(\phi_i^{\mathrm{el}})\right] \times \left[(4\pi A_s/\lambda^2)\cos(\phi_o^{\mathrm{az}})\cos(\phi_o^{\mathrm{el}})\right]$ when $\phi_i^{\mathrm{az}}, \phi_i^{\mathrm{el}}, \phi_o^{\mathrm{az}}, \phi_o^{\mathrm{el}} \in (-\pi/2, \pi/2)$ and $\zeta(\phi_i, \phi_o) = 0$ otherwise; accordingly, at broadside, the entire reflecting area is equal to the sum of the effective apertures of the building elements. Finally, Algorithm 1 is implemented with $K_{\max} = 200$, $\epsilon = 10^{-5}$, and a random initialization.

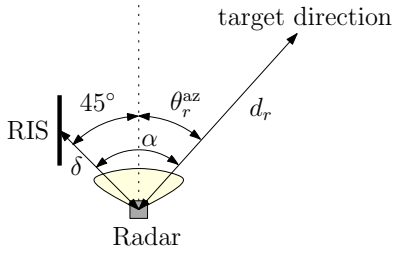

Fig. 1. Considered system geometry.

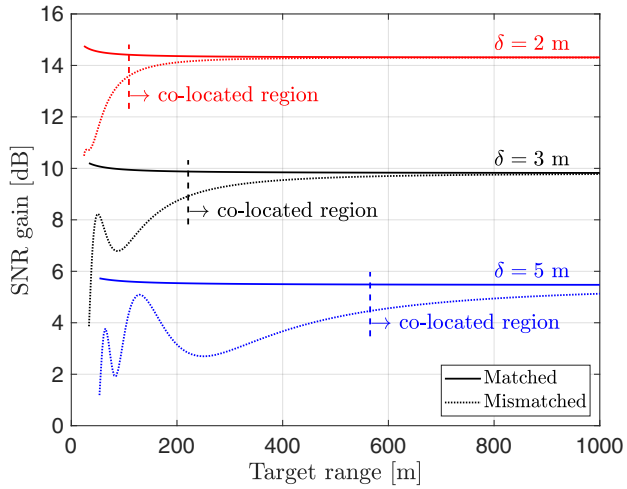

Fig. 2. SNR gain versus the target range, as compared to the case where the radar operates alone, when $\theta_r = 45\,\mathrm{deg}$ and $\delta = 2, 3, 5$ m.

Fig. 2 reports the SNR gain of the RIS-aided radar versus the target range d_r, as compared to the case where the radar operates alone. We consider the performance obtained when the RIS phases are optimized for the true target range (matched case) and for an infinite range (mismatched case), when $\theta_r^{\mathrm{az}} = 45°$ and $\delta = 2, 3, 5$ m. We only plot the corresponding curves when the design assumptions hold (i.e., the target is far enough to be in the far-field of both the radar and the RIS and, also, to offer them the same aspect angle). The following remarks are now in order. The SNR gain gets smaller when the radar-RIS distance increases, as a consequence of the more severe attenuation of the indirect echoes. Let $D_{\max}$ be the maximum distance between any reflecting element and any transmit/receive antenna; then, focusing the RIS at infinity becomes close-to-optimal beyond the range $2D_{\max}^2/\lambda$ (marked by a vertical dashed line), thus

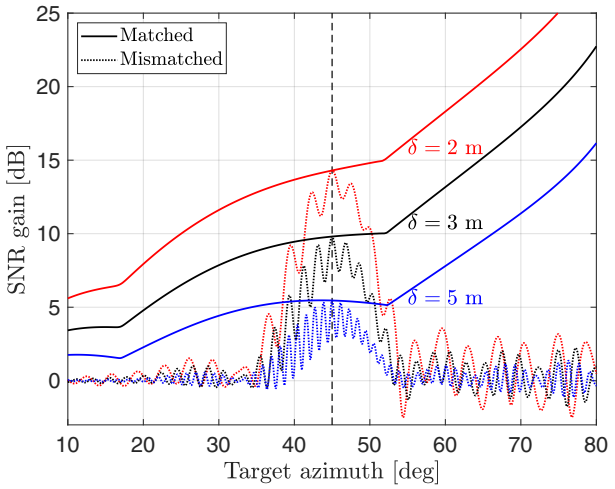

Fig. 3. SNR gain versus the target azimuth, as compared to the case where the radar operates alone, when focusing at infinity and $\delta = 2, 3, 5$ m.

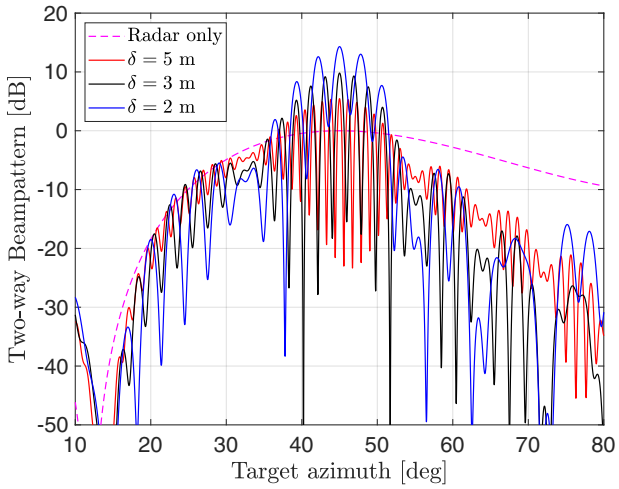

Fig. 4. Two-way azimuth beam-pattern of the RIS-aided radar when focusing towards the azimuth angle $45°$ at infinity and $\delta = 2, 3, 5$ m.

much simplifying the system design. This is a consequence of the fact that a sufficiently far target sees the radar-RIS pair as a unique large array with co-located elements, whereby a plane wave approximation across this augmented aperture remains valid [8]; in particular, in this region the amplitude and the phase imbalance between the direct and direct paths become independent of the range of the focal point, as we have

$$\frac{\bar{\gamma}_r}{\bar{\gamma}_s} \approx \left(\frac{\bar{\mathcal{G}}(\theta_r)}{\bar{\mathcal{G}}(\rho)} \frac{4\pi\delta^2}{\zeta(\omega, \theta_s)} \right)^{1/2} e^{-\mathrm{i}2\pi(\cos\alpha - 1)\delta/\lambda} \tag{8a}$$

$$\frac{\ddot{\gamma}_r}{\ddot{\gamma}_s} \approx \left(\frac{\ddot{\mathcal{G}}(\theta_r)}{\ddot{\mathcal{G}}(\rho)} \frac{4\pi\delta^2}{\zeta(\theta_s, \omega)} \right)^{1/2} e^{-\mathrm{i}2\pi(\cos\alpha - 1)\delta/\lambda} \tag{8b}$$

where α if the angle between the line segments from the radar phase center to the target and from the radar phase center to the RIS phase center (see Fig. 1).

Fig. 3 investigates the achievable SNR gain of the RIS-aided radar as a function of the target azimuth θ_r^{az} when focusing at infinity and $\delta = 2, 3, 5$ m. We report the performance obtained when the RIS phases are optimized for the true target azimuth (matched case) and for a nominal azimuth of $\theta_r = 45°$ (mismatched case); in both cases, the radar receive filter is chosen to maximize the SNR at the inspected direction. Under a matched design, the SNR gain increases when θ_r approaches $90°$, as the RIS offers a larger bi-static RCS towards/from the target. Under a mismatched design, instead, the SNR gain progressively reduces by moving away from $45°$; here the ripple is due to the fact that the direct and indirect echoes do not always add constructively, and, indeed, a small negative gain may even occur occasionally. Overall, the results in Fig. 3 suggest that the system engineer can opportunistically focus the RIS towards a specific direction to locally boost the detection/estimation performance, while the radar transceiver can still keep looking at other regions with acceptable loss. The direction of interest can be for example the one where an alert was previously found [18].

Finally, Fig. 4 shows the two-way azimuth beampattern of the RIS-aided radar for $\delta = 2, 3, 5$ m, when focusing both the RIS phases and the receiver filter towards a nominal azimuth angle of $45°$. It is verified by inspection that a sharper beampattern is obtained when the radar-RIS distance decreases, as compared to the radar-only case. We underline however that the RIS-aided beampattern presents an evident ripple, also in the main-lobe, as the direct and indirect echoes undergo a constructive and a destructive superposition as the target azimuth changes: this makes the proposed design somehow fragile with respect to a small deviation of the true target direction from the nominal pointing direction.

5. CONCLUSIONS

In this work we have considered a monostatic MIMO radar aided by an RIS placed in close proximity, which allows to obtain four paths from the transmitter to the prospective target to the receiver. The analysis has shown that the reflecting surface has the potential to greatly enhance the detection performance of the radar by redirecting/concentrating the radiated power towards/from the target direction.

Future works should investigate more advanced design strategies, which possibly include the optimization of the transmit waveforms and explicitly consider the presence of array calibration errors, capable of producing a two-way beampattern with a reduced ripple in the main-lobe; also, the effect of the clutter should be discussed, and effective adaptive signal processing techniques need to be devised and studied.

6. REFERENCES

[1] E. Basar, M. Di Renzo, J. De Rosny, M. Debbah, M. Alouini, and R. Zhang, "Wireless communications through reconfigurable intelligent surfaces," *IEEE Access*, vol. 7, pp. 116753–116773, 2019.

[2] Y. Liu, X. Liu, X. Mu, T. Hou, J. Xu, M. Di Renzo, and N. Al-Dhahir, "Reconfigurable intelligent surfaces: Principles and opportunities," *IEEE Communications Surveys & Tutorials*, 2021.

[3] W. Lu, B. Deng, Q. Fang, X. Wen, and S. Peng, "Intelligent reflecting surface-enhanced target detection in MIMO radar," *IEEE Sensors Letters*, vol. 5, no. 2, pp. 1–4, Feb. 2021.

[4] S. Buzzi, E. Grossi, M. Lops, and L. Venturino, "Radar target detection aided by reconfigurable intelligent surfaces," *IEEE Signal Processing Letters*, vol. 28, pp. 1315–1319, June 2021.

[5] A. Aubry, A. De Maio, and M. Rosamilia, "RIS-aided radar sensing in N-los environment," in *2021 IEEE 8th International Workshop on Metrology for AeroSpace*, June 2021, pp. 277–282.

[6] S. Buzzi, E. Grossi, M. Lops, and L. Venturino, "Foundations of MIMO radar detection aided by reconfigurable intelligent surfaces," submitted to *IEEE Transactions on Signal Processing*, 2021, https://arxiv.org/pdf/2105.09250.pdf.

[7] E. Fishler, A. Haimovich, R. S. Blum, L. J. Cimini, D. Chizhik, and R. A. Valenzuela, "Spatial diversity in radars – models and detection performance," *IEEE Transactions on Signal Processing*, vol. 54, no. 3, pp. 823–838, Mar. 2006.

[8] W. L. Stutzman and G. A. Thiele, *Antenna Theory and Design*, John Wiley Sons, New York, NY, USA, 3 edition, 1998.

[9] V. Jamali, A. M. Tulino, G. Fischer, R. R. Müller, and R. Schober, "Intelligent surface-aided transmitter architectures for millimeter-wave ultra massive mimo systems," *IEEE Open Journal of the Communications Society*, vol. 2, pp. 144–167, 2021.

[10] M. A. Richards, *Fundamentals of radar signal processing*, McGraw-Hill, New York, NY, USA, 2 edition, 2005.

[11] B. Friedlander, "Localization of signals in the near-field of an antenna array," *IEEE Transactions on Signal Processing*, vol. 67, no. 15, pp. 3885–3893, Aug. 2019.

[12] S. M. Kay, *Fundamental of Statistical Signal Processing: Estimation Theory*, vol. I, Prentice Hall, 1993.

[13] S. M. Kay, *Fundamental of Statistical Signal Processing: Detection Theory*, vol. II, Prentice Hall, 1993.

[14] E. Grossi, M. Lops, and L. Venturino, "A new look at the radar detection problem," *IEEE Transactions on Signal Processing*, vol. 64, no. 22, pp. 5835–5847, Nov. 2016.

[15] S. W. Ellingson, "Path loss in reconfigurable intelligent surface-enabled channels," *arXiv:1912.06759*, 2019.

[16] W. Tang, M. Z. Chen, X. Chen, J. Y. Dai, Y. Han, M. Di Renzo, Y. Zeng, S. Jin, Q. Cheng, and T. J. Cui, "Wireless communications with reconfigurable intelligent surface: Path loss modeling and experimental measurement," *IEEE Transactions on Wireless Communications*, vol. 20, no. 1, pp. 421–439, Jan. 2021.

[17] W. Tang, X. Chen, M. Z. Chen, J. Y. Dai, Y. Han, M. D. Renzo, S. Jin, Q. Cheng, and T. J. Cui, "Path loss modeling and measurements for reconfigurable intelligent surfaces in the millimeter-wave frequency band," *arXiv:2101.08607*, 2021.

[18] E. Grossi, M. Lops, and L. Venturino, "Two-step sequential detection in agile-beam radars: Performance and tradeoffs," *IEEE Transactions on Aerospace and Electronic Systems*, vol. 53, no. 5, pp. 2199–2213, Oct. 2017.